RSC Advances

PAPER

View Article Online
View Journal | View Issue

Cite this: *RSC Adv.*, 2017, **7**, 47219

Isostructural functionalization by –OH and –NH_2: different contributions to CO_2 adsorption†

Zhiyong Lu,*[a] Yue Xing,[a] Liting Du,[b] Haiyan He,[a] Jianfeng Zhang*[a] and Cheng Hang[c]

Received 18th September 2017
Accepted 29th September 2017

DOI: 10.1039/c7ra10369g

rsc.li/rsc-advances

Two isostructural *mfj*-type metal–organic frameworks, $[Cu_2(ABDPB)(H_2O)]_n$ (HHU-3, HHU for Hohai University; H_4ABDPB for 5-amino-1,3-bis(3,5-dicarboxylphenyl)-benzene) and $[Cu_2(OBDPB)(H_2O)]_n$ (HHU-4; H_4OBDPB for 5-hydroxyl-1,3-bis(3,5-dicarboxylphenyl)-benzene) were successfully synthesized by V-shaped tetracarboxylic ligand with amino and hydroxyl groups, respectively. Compared with the prototypical MOF, PCN-306, both MOFs exhibit obviouse decreases in BET surface area and pore volume, with the values of 2354 $m^2\ g^{-1}$ and 0.920 $cm^3\ g^{-1}$ for HHU-3, and 2353 $m^2\ g^{-1}$ and 0.954 $cm^3\ g^{-1}$ for HHU-4. Although both functional groups are believed to be effective in strengthen CO_2 interactions with the framework, in this type of MOF, amino group works better due to its basic nature. Meanwhile, the decoration of amino groups grafted HHU-3 high CO_2 adsorption capacity (25.6 wt% at 1 bar and 273 K) and high CO_2 selectivity ($S_{CO_2/N_2} = 129$).

Introduction

Metal–organic frameworks (MOFs), as promising porous materials, have shown great potential in gas storage and separation due to their large surface area and high porosity.[1–11] Compared with traditional porous materials, the feasibility of structural tunability is a great advantage of MOFs. Various functional groups can be intentionally introduced into frameworks *via* either ligand-design or post-synthetic modification to achieve high performance.[12–16] Practically, both of them show their own pros and cons. Sharp decrease in pore volume generally happens in the functionalization reactions of post-synthetic process, and therefore leads to the declines of gas adsorption capacity. Besides, the completeness of functionalization cannot be easily attained.[17] Pre-design modification shows its advantage in obtaining the totally functionalized MOF. However, due to the chemical/physical activity of some functional groups, it requires a structural-stable prototypical MOF that can resist these groups from interfering the formation of the desired MOF.[18,19]

Mfj-type MOF is a good platform for functionalization towards high performance in gas adsorption, as illustrated by PCN-306 and its analogues, in which the introduction of different functional groups by pre-synthetic method seldom led to a structural change.[20–22] Based upon this type of MOF, in this contribution, we managed to decorate the channels in PCN-306 by two different polar groups, –NH_2 and –OH (Scheme 1), both of which are regarded to be effective in strengthening CO_2-framework interactions.[23–25] The functional groups were selected on the basis of two points: (a) similar size, which avoids the influence of narrow pore effect induced by different pore sizes; (b) different acid-base property makes the comparison of their effect on gas adsorption more specific. Compared with the prototypical MOF PCN-306, the resulted two *mfj*-type MOF $[Cu_2(ABDPB)(H_2O)_2]_n$ (HHU-3, HHU for Hohai University; H_4ABDPB for 5-amino-1,3-bis(3,5-dicarboxylphenyl)-benzene) and $[Cu_2(OBDPB)(H_2O)_2]_n$ (HHU-4; H_4OBDPB for 5-hydroxyl-1,3-bis(3,5-dicarboxylphenyl)-benzene) exhibit slight decreases in BET surface area, with the values of 2354 $m^2\ g^{-1}$ and 2353 $m^2\ g^{-1}$ respectively. Although both of them are polar functional groups, which are expected to be effective in CO_2 adsorption in MOFs,

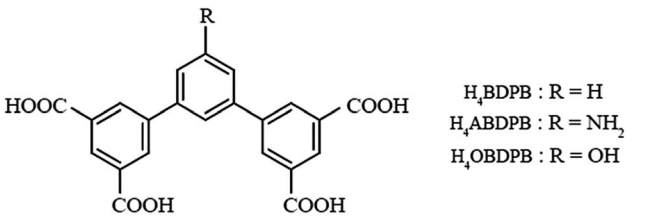

Scheme 1 Ligands-functionalization by hydroxyl and amino groups.

[a]College of Mechanics and Materials, Hohai University, Nanjing 210098, China. E-mail: johnlook1987@gmail.com; jfzhang_sic@163.com

[b]Advanced Analysis and Testing Center, Nanjing Forestry University, Nanjing 210037, China

[c]State Key Laboratory of Coordination Chemistry, Nanjing University, Nanjing 210093, China

† Electronic supplementary information (ESI) available: Experimental details, PXRD patterns, crystallographic data, additional gas adsorption isotherms, heat of adsorption, TG curves. CCDC 1566591 and 1566592. For ESI and crystallographic data in CIF or other electronic format see DOI: 10.1039/c7ra10369g

amine groups obviously work better than hydroxyl groups. The decoration of amino groups grafted HHU-3 high CO_2 adsorption capacity (25.6 wt% at 1 bar and 273 K) and high CO_2 selectivity ($S_{CO_2/N_2} = 129$).

Experimental

Materials and methods

All chemical reagents were obtained from commercial sources and, unless otherwise noted, were used as received without further purification. Elemental analyses (C, H, and N) were performed on a Perkin-Elmer 240 analyzer. The IR spectra were recorded in the 400–4000 cm^{-1} on a Bruker VERTEX 80V spectrometer using KBr pellets. ^1H NMR spectra were recorded on a Bruker DRX-500 spectrometer with tetramethylsilane as an internal reference. Thermal gravimetric analyses (TGA) were performed under N_2 atmosphere (100 mL min^{-1}) with a heating rate of 5 °C min^{-1} using a 2960 SDT thermogravimetric analyzer. Powder X-ray diffraction (PXRD) data were collected on a Bruker D8 ADVANCE X-ray diffractometer with Cu/Kα radiation.

Gas sorption measurements

Low-pressure gas sorption measurements were carried out using a Micromeritics ASAP 2020 surface area and pore size analyzer up to saturated pressure at different temperatures. Before the gas sorption measurement, more than 200 mg as-synthesized sample (PCN-306/HHU-3/HHU-4) was washed with DMF and methanol (acetone for PCN-306), respectively. Fresh anhydrous methanol (acetone for PCN-306) was then added, and the sample was allowed to soak for 3 days for solvent-exchange. During this period, methanol (acetone for PCN-306) was refreshed every 8 hours. After then, the sample was charged into a sample tube and activated at certain temperature (120 °C for PCN-306, 80 °C for HHU-3, and 90 °C for HHU-4) for 12 hours under vacuum.

X-ray collection and structure determination

Single crystal suitable for X-ray structure determination were selected and sealed in a capillary under a microscope. The X-ray diffraction intensity data were measured on a BRUKER D8 VENTURE PHOTON diffractometer at room temperature using graphite monochromated Mo/Kα radiation ($\lambda = 0.71073$ Å). Data reduction was made with the Bruker Saint program. The structures were solved by direct methods and refined with full-matrix least squares technique using the SHELXTL package. Non-hydrogen atoms were refined with anisotropic displacement parameters during the final cycles. Hydrogen atoms were placed in calculated positions with isotropic displacement parameters set to 1.2 × U_{eq} of the attached atom. The unit cell includes a large region of disordered solvent molecules, which could not be modeled as discrete atomic sites. We employed PLATON/SQUEEZE to calculate the diffraction contribution of the solvent molecules and, thereby, to produce a set of solvent-free diffraction intensities; structures were then refined again using the data generated. Crystal data and refinement conditions are shown in Table S1.† The crystal data for HHU-3 and HHU-4 have been deposited in CSD database, and labeled as 1566591 and 1566592, respectively.

Synthesis and characterization

Syntheses of organic linker 1,3-bis(3,5-dicarboxylphenyl)-benzene (H_4BDPB), 5-amino-1,3-bis(3,5-dicarboxylphenyl)-benzene (H_4ABDPB), and 5-hydroxyl-1,3-bis(3,5-dicarboxylphenyl)-benzene (H_4OBDPB) (Scheme 1). Details of their synthetic procedure are given in the ESI.†

H_4ABDPB. ^1H NMR (500 MHz, DMSO-d_6, δ ppm): 13.37 (brs, 4H, COOH), 8.47 (s, 2H, ArH), 8.42 (s, 4H, ArH), 7.19 (s, 1H, ArH), 7.04 (s, 2H, ArH), 5.76 (brs, 2H, NH). Selected FTIR (neat, cm^{-1}): 3399, 2921, 1702, 1599, 1380, 1236, 909, 866, 760, 675, 639.

HHU-3. A mixture of H_4ABDPB (5.05 mg, 0.012 mmol) and $CuCl_2 \cdot 2H_2O$ (13.6 mg, 0.08 mmol) was dissolved in DMF/H_2O (2 mL, 5: 1, v/v) in a screw-capped vial. A concentrated HNO_3 (0.03 mL) (65%, aq.) was added to the mixture, the vial was capped and placed in an oven at 65 °C for one day. The resulting dark-green pyramid-shaped crystals were filtered and washed with DMF several times to give HHU-3 materials. Yield: 76%. Elemental analysis: calcd for activated Cu_2(ABDPB), (%): C, 48.44; H, 2.02; N, 2.57; found: C, 48.16; H, 2.27; N, 2.83.‡

H_4OBDPB. ^1H NMR (500 MHz, DMSO-d_6, δ ppm): 13.62 (brs, 4H, COOH), 8.51 (s, 2H, ArH), 8.47 (s, 4H, ArH), 8.05 (s, 1H, OH), 7.81 (d, $^4J_{H-H} = 7.5$ Hz, 2H, ArH), 7.67 (t, $^4J_{H-H} = 7.5$ Hz, 1H, ArH). Selected FTIR (neat, cm^{-1}): 3420, 3083, 2525, 1705, 1598, 1444, 1385, 1203, 914, 851, 756, 673, 636.

HHU-4. A mixture of H_4OBDPB (5.06 mg, 0.012 mmol) and $CuCl_2 \cdot 2H_2O$ (6.8 mg, 0.04 mmol) was dissolved in DMF/H_2O (2 mL, 5: 1, v/v) in a screw-capped vial. A concentrated HNO_3 (0.05 mL) (65%, aq.) was added to the mixture, the vial was capped and placed in an oven at 65 °C for one day. The resulting blue pyramid-shaped crystals were filtered and washed with DMF several times to give HHU-4 materials. Yield: 64%. Elemental analysis: calcd for activated Cu_2(OBDPB), (%): C, 48.35; H, 1.83; N, 0; found: C, 48.01; H, 2.02; N, 0.03.

H_4BDPB. ^1H NMR (500 MHz, DMSO-d_6, δ ppm): 13.56 (brs, 4H, COOH), 8.51 (s, 2H, ArH), 8.47 (s, 4H, ArH), 8.05 (s, 1H, ArH), 7.81 (d, $J = 5$ Hz, 2H, ArH), 7.68 (d, $J = 5$ Hz, 1H, ArH). Selected FTIR (neat, cm^{-1}): 3405, 2991, 1700, 1599, 1440, 1234, 905, 755, 675, 633.

PCN-306. A mixture of H_4BDPB (4.86 mg, 0.012 mmol) and $CuCl_2 \cdot 2H_2O$ (13.6 mg, 0.08 mmol) was dissolved in DMF/H_2O (2 mL, 5: 1, v/v) in a screw-capped vial. A concentrated HNO_3 (0.05 mL) (65%, aq.) was added to the mixture, the vial was

‡ Crystal data for HHU-3: $C_{66}H_{33}Cu_6N_3O_{30} \cdot x$(solv.), $M = 1729.25$, orthorhombic, $Cmc2_1$, $a = 24.600(2)$ Å, $b = 33.412(3)$ Å, $c = 18.478(2)$ Å, $\alpha = \beta = \gamma = 90°$, $V = 15\,188(2)$ Å^3, $Z = 4$, $D_c = 0.756$ g cm^{-3}, GOF = 0.898 based on F^2, final $R_1 = 0.0604$, w$R_2 = 0.1201$ [for 15 966 data $I > 2\sigma(I)$]; data for structure was treated with Squeeze. Crystal data for HHU-4: $C_{66}H_{30}Cu_6O_{33} \cdot x$(solv.), $M = 1732.20$, orthorhombic, $Cmcm$, $a = 24.6748(11)$ Å, $b = 33.5109(15)$ Å, $c = 18.4547(11)$ Å, $\alpha = \beta = \gamma = 90°$, $V = 15\,259.7(13)$ Å^3, $Z = 4$, $D_c = 0.754$ g cm^{-3}, GOF = 1.021 based on F^2, final $R_1 = 0.0751$, w$R_2 = 0.1828$ [for 6843 data $I > 2\sigma(I)$]; data for structure was treated with Squeeze.

capped and placed in an oven at 65 °C for two days. The resulting blue pyramid-shaped crystals were filtered and washed with DMF several times to give PCN-306 materials. Yield: 53%. Elemental analysis: calcd for activated Cu_2(BDPB), (%): C, 49.91; H, 1.70; N, 0.00; found: C, 49.65; H, 1.91; N, 0.05.

Results and discussion

Single-crystal X-ray diffraction analysis reveals that HHU-4 crystallizes in orthorhombic space group *Cmcm*. The asymmetric unit of HHU-4 consists of three crystallographically unique Cu^{2+} ions (Cu1, Cu2, and Cu3 with the occupation of 1, 1/4, and 1/4, respectively), one half and a quarter OBDPB-ligand and three coordinated water molecules (Fig. S1†). HHU-3 crystallizes in a different orthorhombic space group $Cmc2_1$, which has less symmetric elements than *Cmcm*. Therefore, the asymmetric unit of HHU-3 consists of more moieties, with four crystallographically unique Cu^{2+} ions, one and a half ABDPB-ligand and four coordinated water molecules. Although they are in different space groups due to different torsion angles, the structures of HHU-3 and HHU-4 are isostructural to PCN-306, as shown in Fig. 1 by their PXRD patterns and crystal structures. The structure of both HHU-3 and HHU-4 contains two types of ligands with different dihedral angles between central and terminal benzene rings. As illustrated in Fig. 2, the dihedral angles between central and terminal benzene rings in HHU-3 are about 38.0°, 47.7° and 52.8°, while the dihedral angels in HHU-4 are approximately 43.4° and 52.7°. Bridged by these ligands, all the paddlewheel dinuclear Cu clusters [$Cu_2(COO)_4$] are assembled into the same (3,3,4,4)-c 4-nodal *mfj*-type net in both HHU-3 and HHU-4 if paddlewheel Cu clusters are simplified as 4-connected nodes and ligands as two 3-connected nodes (Fig. S2 and S3†). Obviously, due to functionalization, windows along *c* axis were narrowed from 9 Å to 6 Å while windows along *a* axis exhibit no obvious change (Fig. 1a and b). By PLATON, the total potential solvent accessible volume of HHU-3 and HHU-4 were calculated to be 70.8% and 69.8%. Therefore, from the perspective of volume occupancy, the introduction of $-NH_2$ and –OH costs almost the same pore volume.

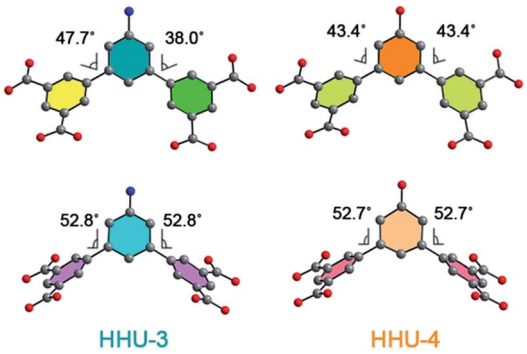

Fig. 2 Two types of ligands in HHU-3 and HHU-4.

In order to investigate the effect of functional groups, the permanent porosities of HHU-3 and HHU-4 were determined by N_2 adsorption measurements at 77 K. For a clear comparison, we also measured the N_2 adsorption of PCN-306. Before measurements, the solvent-exchanged samples were evacuated at certain temperature for 12 hours, with crystallinity remained after solvent removal (Fig. S4–S6†). BET analysis reveals obvious decreases in surface area of functionalized MOFs. As shown in Fig. 3, the N_2 uptake amount of PCN-306 at $P/P_0 = 1$ is 690.3 $cm^3\ g^{-1}$, which agrees quite well with that reported by Zhou group.[20] Functionalization caused a slight decrease of N_2 uptake amount in HHU-3 and HHU-4, with the value of

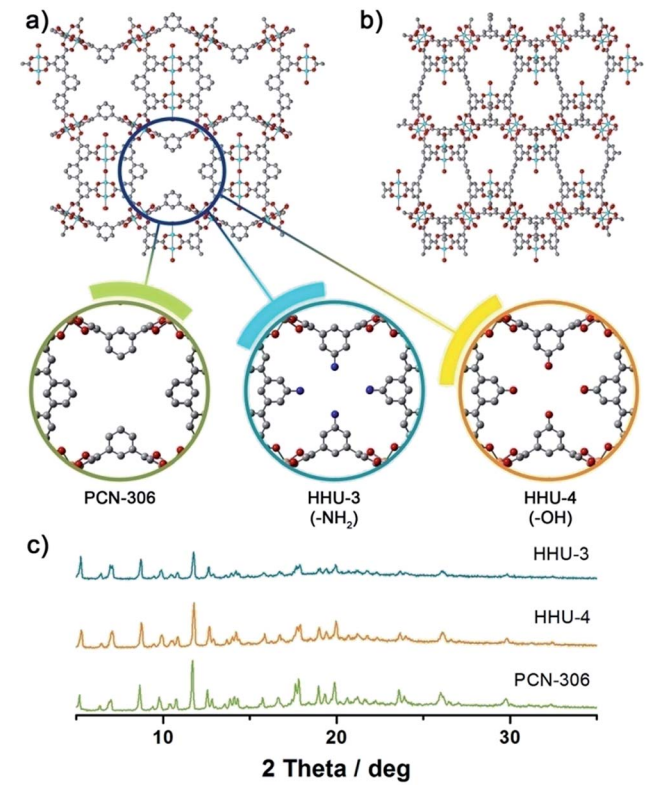

Fig. 1 Functionalizing PCN-306 by –OH and $-NH_2$ group. (a) and (b) are channels along *c* axis and *a* axis; (c) is the PXRD patterns of as-synthesized samples of PCN-306, HHU-3, and HHU-4.

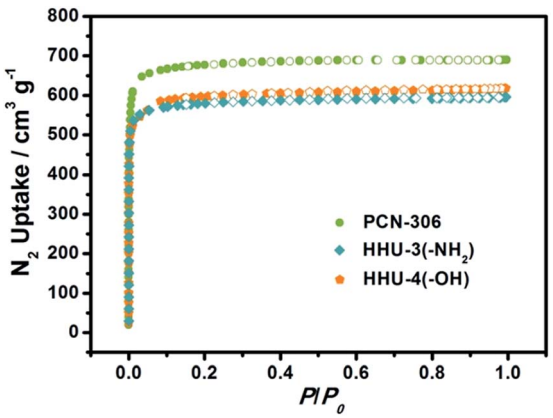

Fig. 3 N_2 adsorption isotherms of PCN-306, HHU-3 and HHU-4 at 77 K.

596.0 $cm^3\ g^{-1}$ and 618.6 $cm^3\ g^{-1}$, respectively. Based on N_2 isotherms, the BET surface areas of PCN-306, HHU-3 and HHU-4 were calculated to be 2772 $m^2\ g^{-1}$, 2354 $m^2\ g^{-1}$, and 2353 $m^2\ g^{-1}$, respectively. If monolayer coverage of N_2 is assumed, the Langmuir surface areas of PCN-306, HHU-3 and HHU-4 were estimated to be 3003 $m^2\ g^{-1}$, 2570 $m^2\ g^{-1}$, and 2656 $m^2\ g^{-1}$, respectively. As expected, the total pore volume decreases from 1.066 $cm^3\ g^{-1}$ in PCN-306 to 0.920 $cm^3\ g^{-1}$ in HHU-3, and 0.954 $cm^3\ g^{-1}$ in HHU-4, consistent with the size of functional groups.

Both the crystal structures and N_2 adsorption measurements reveal that $-NH_2$ and $-OH$ have similar size, which help us exclude the pore-size effect on gas adsorption caused by functional groups with different sizes. Therefore, we measured the H_2 adsorption capacities of both HHU-3 and HHU-4, as well as their prototypical MOF, PCN-306. As shown in Fig. 4a, the H_2 adsorption capacities of PCN-306, HHU-3, and HHU-4 at 1 bar and 77 K are 2.61 wt%, 2.46 wt%, and 2.36 wt%, respectively. PCN-306 shows the highest H_2 adsorption capacity at 77 K, which is consistent with its large surface area and pore volume. After functionalization, the decline of surface area and pore volume lead to the decrease of H_2 adsorption capacity in HHU-3 and HHU-4. Based upon the isotherms measured at 77 K and 87 K, the H_2 adsorption enthalpies of PCN-306, HHU-3, and HHU-4 were calculated. As shown in Fig. 4b, the zero-coverage H_2 adsorption enthalpies of HHU-3 and HHU-4 are 6.41 kJ mol^{-1}, 6.60 kJ mol^{-1}, which are slightly lower than that of PCN-306 (6.65 kJ mol^{-1}). Therefore, the introduction of polar functional groups do not benefit H_2 adsorption in *mfj*-type MOFs, but causes the decrease of surface area and pore volume which closely correlate with hydrogen uptake capacity.

Since we deliberately grafted polar functional groups in MOF materials, an improvement in CO_2 adsorption was expected. Thus, we measured the CO_2 adsorption of each MOF, as shown in Fig. 4c. Compared with the prototype MOF, PCN-306, the CO_2 adsorption capacity of the amino-functionalized MOF, HHU-3, exhibits an obvious improvement. At 1 bar and 273 K, the CO_2 uptake amount of HHU-3 is 175 $cm^3\ g^{-1}$ (25.6 wt%), which is higher than most of its iso-structural analogues (Table 1) and meanwhile much higher than that of some typical MOFs, such as CAU-1 (ref. 26) (161 $cm^3\ g^{-1}$), SNU-4 (ref. 27) (20.6 wt%) and MOF-5 (ref. 28) (6.2 wt%). This value is also quit comparable with that of Cu-EBTC[29] (25.9 wt%). The hydroxyl-functionalized MOF, HHU-4, however, exhibits a lower adsorption capacity with the value of 164.7 $cm^3\ g^{-1}$ (24.4 wt%) at 1 bar. Similar behavior was also observed in CO_2 isotherms of HHU-3, PCN-306, and HHU-4 at 298 K (Fig. 4c), with the values of 93.0 $cm^3\ g^{-1}$ (15.4 wt%), 84.7 $cm^3\ g^{-1}$ (14.3 wt%), and

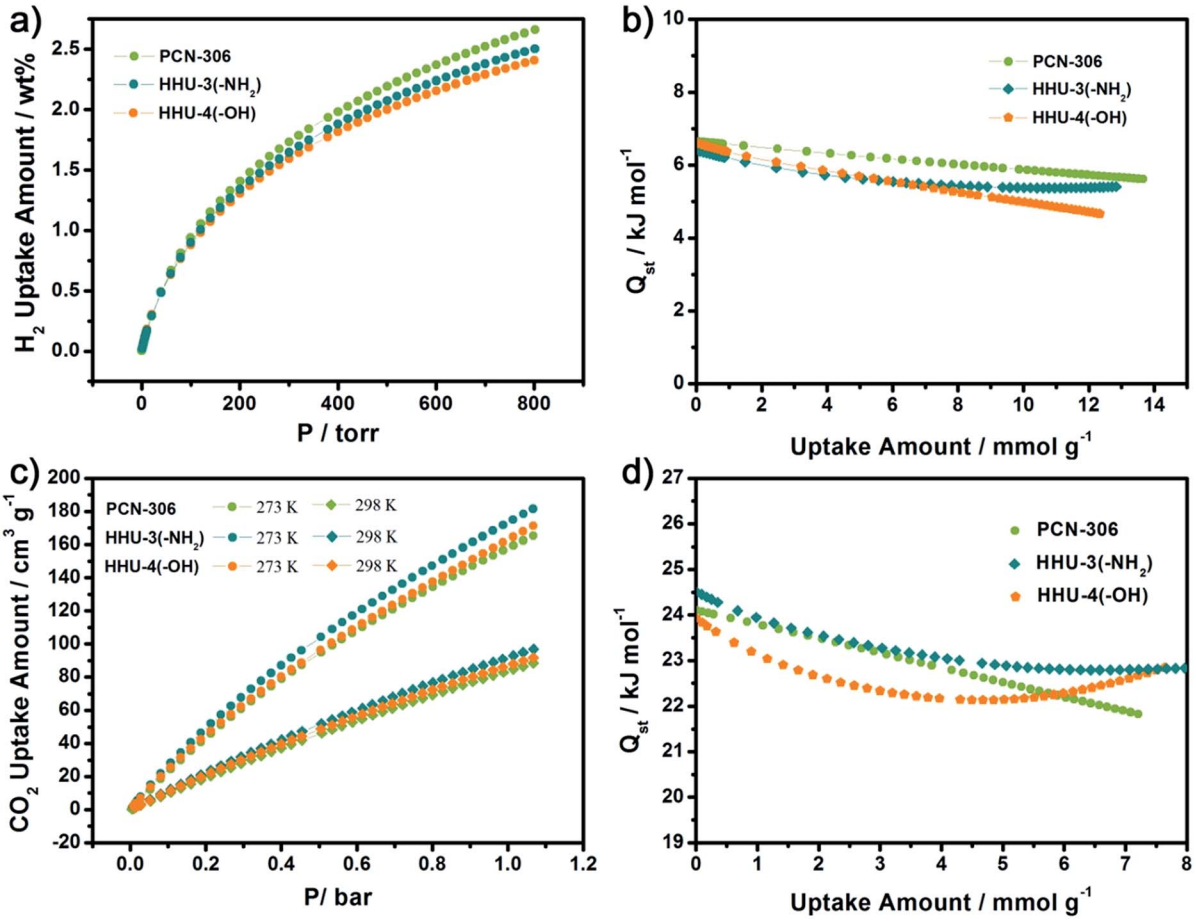

Fig. 4 (a) H_2 adsorption isotherms for PCN-306, HHU-3 and HHU-4 at 77 K; (b) H_2 adsorption enthalpies of PCN-306, HHU-3 and HHU-4; (c) CO_2 adsorption isotherms for PCN-306, HHU-3 and HHU-4 at 273 K and 298 K; (d) CO_2 adsorption enthalpies of PCN-306, HHU-3 and HHU-4.

Table 1 Pore characteristics and CO_2 adsorption capacities for selected iso-structural analogues

MOFs	$S_{Langmuir}$ [m^2 g^{-1}]	V_{pore} [cm^3 g^{-1}]	Q_{st} [kJ mol^{-1}]	CO_2 at 273 K [wt%]
PCN-306 (–H)	2929[a]/3003[b]	1.043[a]/1.066[b]	24.0[a]/24.1[b]	22.9[a]/23.8[b]
HHU-3 (–NH_2)	2570	0.920	24.6	25.6
PCN-305 (–N)	2599	0.926	23.8	23.2
PCN-307 (–CH_3)	2235	0.808	22.8	23.2
HHU-4 (–OH)	2656	0.954	23.9	24.4
PCN-308 (–CF_3)	2234	0.810	22.2	24.8

[a] According to ref. 20. [b] Data collected in this article.

88.0 cm^3 g^{-1} (14.7 wt%) at 1 bar, respectively. Thus the adsorption enthalpy of CO_2 adsorption for each MOF was calculated by the virial method, using experimental isotherm data at 273 K and 298 K. As shown in Fig. 4d, the CO_2 adsorption enthalpies at zero-coverage for PCN-306, HHU-3 and HHU-4 were 24.1 kJ mol^{-1}, 24.6 kJ mol^{-1} and 23.9 kJ mol^{-1}, respectively. Although the improvement is not significant in zero-coverage, the CO_2 adsorption enthalpy of HHU-3 is higher than that of PCN-306 at all loading range, while that of HHU-4 is lower than that of PCN-306 at most range. From the perspective of enhancing CO_2 adsorption capacity, amino group performs much better than hydroxyl group due to its basic property which is favored by CO_2 molecules.

As amino group has positive effect on CO_2 adsorption, we further compared the CO_2 selectivities of HHU-3 and PCN-306 over N_2 *via* the Ideal Adsorption Solution Theory (IAST). As shown Fig. 5, the CO_2 selectivity of PCN-306 towards N_2 is 76 at 1 bar in the case of $CO_2/N_2 = 15:85$ gas mixtures. For HHU-3, obvious improvement in CO_2/N_2 selectivity was observed, with the value of 129 at 1 bar. Meanwhile, this value is much higher than some well-known MOFs such as Fe-BTT[30,31] (CO_2/N_2: 61), Cu-TDPAT[30] (CO_2/N_2: 88), and quite comparable with en-CuBTTri[32] (CO_2/N_2: 143), SIFSIX-2-Cu-i[5] (CO_2/N_2: 140), and Mg-MOF-74 (ref. 33) (CO_2/N_2: 148.1), indicating a high CO_2 selectivity. The incorporation of amino groups benefits CO_2 adsorption, therefore contributes to a higher CO_2 selectivity compared to the prototypical MOF.

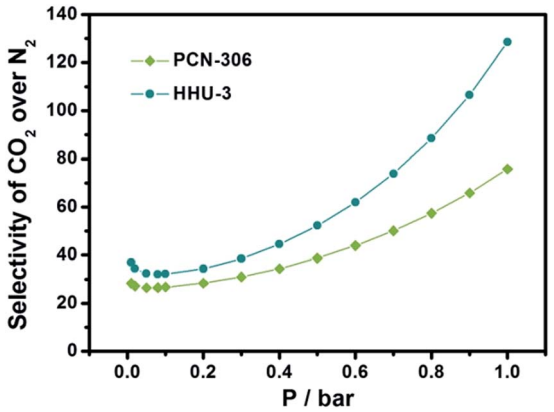

Fig. 5 CO_2/N_2 selectivity of HHU-3 and PCN-306 at 273 K by IAST.

Conclusions

In summary, based upon a structural-stable *mfj*-type MOF, PCN-306, a pre-synthetic approach of functionalization was applied and its amino- and hydroxyl-functionalized analogues were obtained respectively. Due to comparable size of functional groups, HHU-3 and HHU-4 show similar decreases in both BET surface area and pore volume, which cause decline in their capacities for H_2 adsorption. Although both amino and hydroxyl groups are regarded to be effective in strengthen CO_2 interactions with the framework, in this type of MOF, amino group works better than hydroxyl group due to its basic nature favoured by CO_2 molecules. The high CO_2 uptake amount among *mfj*-type MOFs and high CO_2 selectivity make HHU-3 one of potential candidates for CO_2 capture.

Conflicts of interest

There are no conflicts to declare.

Acknowledgements

This work was supported by the Natural Science Fund of Jiangsu Province (Grant No. BK20150798, BK20140968, BK20161506 and BK20160857), the National Natural Science Foundation of China (Grant No. 21601047 and 21501094), the Fundamental Research Funds for the Central Universities (Grant No. 2015B12014) and Jiangsu Doctor Program (Grant No. B15065).

Notes and references

1 P. M. Bhatt, Y. Belmabkhout, A. Cadiau, K. Adil, O. Shekhah, a. shkurenko, L. J. Barbour and M. Eddaoudi, *J. Am. Chem. Soc.*, 2016, **138**, 9301–9307.
2 Y. He, W. Zhou, G. Qian and B. Chen, *Chem. Soc. Rev.*, 2014, **43**, 5657–5678.
3 X. Zhao, X. Bu, Q. G. Zhai, H. Tran and P. Feng, *J. Am. Chem. Soc.*, 2015, **137**, 1396–1399.
4 T. F. Liu, D. Feng, Y. P. Chen, L. Zou, M. Bosch, S. Yuan, Z. Wei, S. Fordham, K. Wang and H. C. Zhou, *J. Am. Chem. Soc.*, 2015, **137**, 413–419.
5 P. Nugent, Y. Belmabkhout, S. D. Burd, A. J. Cairns, R. Luebke, K. Forrest, T. Pham, S. Ma, B. Space, L. Wojtas, M. Eddaoudi and M. J. Zaworotko, *Nature*, 2013, **495**, 80–84.

6 X. Zhao, X. Bu, E. T. Nguyen, Q. G. Zhai, C. Mao and P. Feng, *J. Am. Chem. Soc.*, 2016, **138**, 15102–15105.
7 O. Shekhah, Y. Belmabkhout, Z. Chen, V. Guillerm, A. Cairns, K. Adil and M. Eddaoudi, *Nat. Commun.*, 2014, **5**, 4228.
8 C. E. Wilmer, O. K. Farha, T. Yildirim, I. Eryazici, V. Krungleviciute, A. A. Sarjeant, R. Q. Snurr and J. T. Hupp, *Energy Environ. Sci.*, 2013, **6**, 1158.
9 D. Wang, B. Liu, S. Yao, T. Wang, G. Li, Q. Huo and Y. Liu, *Chem. Commun.*, 2015, **51**, 15287–15289.
10 I. Senkovska and S. Kaskel, *Chem. Commun.*, 2014, **50**, 7089–7098.
11 Z. Lu, J. Zhang, J. Duan, L. Du and C. Hang, *J. Mater. Chem. A*, 2017, **5**, 17287–17292.
12 A. L. Grzesiak, F. J. Uribe, N. W. Ockwig, O. M. Yaghi and A. J. Matzger, *Angew. Chem., Int. Ed.*, 2006, **45**, 2553–2556.
13 H.-M. Wen, G. Chang, B. Li, R.-B. Lin, T.-L. Hu, W. Zhou and B. Chen, *Cryst. Growth Des.*, 2017, **17**, 2172–2177.
14 P. V. Dau and S. M. Cohen, *Chem. Commun.*, 2014, **50**, 12154–12157.
15 R. Banerjee, H. Furukawa, D. Britt, C. Knobler, M. O'Keeffe and O. M. Yaghi, *J. Am. Chem. Soc.*, 2009, **131**, 3875–3877.
16 N. H. Alsmail, M. Suyetin, Y. Yan, R. Cabot, C. P. Krap, J. Lu, T. L. Easun, E. Bichoutskaia, W. Lewis, A. J. Blake and M. Schroder, *Chem.–Eur. J.*, 2014, **20**, 7317–7324.
17 X. Kong, H. Deng, F. Yan, J. Kim, J. A. Swisher, B. Smit, O. M. Yaghi and J. A. Reimer, *Science*, 2013, **341**, 882–885.
18 R. K. Deshpande, J. L. Minnaar and S. G. Telfer, *Angew. Chem., Int. Ed.*, 2010, **49**, 4598–4602.
19 Z. Wang and S. M. Cohen, *Chem. Soc. Rev.*, 2009, **38**, 1315–1329.
20 Y. Liu, J. R. Li, W. M. Verdegaal, T. F. Liu and H. C. Zhou, *Chem.–Eur. J.*, 2013, **19**, 5637–5643.
21 Z. Lu, L. Du, K. Tang and J. Bai, *Cryst. Growth Des.*, 2013, **13**, 2252–2255.
22 L. Du, Z. Lu, L. Xu and J. Zhang, *RSC Adv.*, 2017, **7**, 21268–21272.
23 Y. Zhao, H. Wu, T. J. Emge, Q. Gong, N. Nijem, Y. J. Chabal, L. Kong, D. C. Langreth, H. Liu, H. Zeng and J. Li, *Chem.–Eur. J.*, 2011, **17**, 5101–5109.
24 K. Sumida, D. L. Rogow, J. A. Mason, T. M. McDonald, E. D. Bloch, Z. R. Herm, T. H. Bae and J. R. Long, *Chem. Rev.*, 2012, **112**, 724–781.
25 Q. Yang, A. D. Wiersum, P. L. Llewellyn, V. Guillerm, C. Serre and G. Maurin, *Chem. Commun.*, 2011, **47**, 9603–9605.
26 X. Si, C. Jiao, F. Li, J. Zhang, S. Wang, S. Liu, Z. Li, L. Sun, F. Xu, Z. Gabelica and C. Schick, *Energy Environ. Sci.*, 2011, **4**, 4522.
27 Y. G. Lee, H. R. Moon, Y. E. Cheon and M. P. Suh, *Angew. Chem., Int. Ed.*, 2008, **47**, 7741–7745.
28 K. S. Walton, A. R. Millward, D. Dubbeldam, H. Frost, J. J. Low, O. M. Yaghi and R. Q. Snurr, *J. Am. Chem. Soc.*, 2008, **130**, 406–407.
29 Y. Hu, S. Xiang, W. Zhang, Z. Zhang, L. Wang, J. Bai and B. Chen, *Chem. Commun.*, 2009, 7551–7553.
30 Z. Zhang, Z. Li and J. Li, *Langmuir*, 2012, **28**, 12122–12133.
31 K. Sumida, S. Horike, S. S. Kaye, Z. R. Herm, W. L. Queen, C. M. Brown, F. Grandjean, G. J. Long, A. Dailly and J. R. Long, *Chem. Sci.*, 2010, **1**, 184.
32 A. Demessence, D. M. D'Alessandro, M. L. Foo and J. R. Long, *J. Am. Chem. Soc.*, 2009, **131**, 8784–8786.
33 J. A. Mason, K. Sumida, Z. R. Herm, R. Krishna and J. R. Long, *Energy Environ. Sci.*, 2011, **4**, 3030.